

Modeling of graphene wrapped indium antimonide nanowire as thermo-optical waveguide

Original

Modeling of graphene wrapped indium antimonide nanowire as thermo-optical waveguide / Sajid, Muhammad; Yaqoob, Muhammad Zeshan; Alkanhal, Majeed A S; Ghaffar, Abdul; Ali, Ahtisham; Khan, Yasin. - In: MATERIALS RESEARCH EXPRESS. - ISSN 2053-1591. - 12:3(2025), pp. 1-16. [[10.1088/2053-1591/adb8a4](https://doi.org/10.1088/2053-1591/adb8a4)]

Availability:

This version is available at: 11583/2998263 since: 2025-03-13T10:09:12Z

Publisher:

IOP Publishing

Published

DOI:[10.1088/2053-1591/adb8a4](https://doi.org/10.1088/2053-1591/adb8a4)

Terms of use:

This article is made available under terms and conditions as specified in the corresponding bibliographic description in the repository

Publisher copyright

(Article begins on next page)

ACCEPTED MANUSCRIPT • OPEN ACCESS

Modeling of Graphene Wrapped Indium Antimonide Nanowire as thermo-optical Waveguide

To cite this article before publication: Muhammad Sajid *et al* 2025 *Mater. Res. Express* in press <https://doi.org/10.1088/2053-1591/adb8a4>

Manuscript version: Accepted Manuscript

Accepted Manuscript is “the version of the article accepted for publication including all changes made as a result of the peer review process, and which may also include the addition to the article by IOP Publishing of a header, an article ID, a cover sheet and/or an ‘Accepted Manuscript’ watermark, but excluding any other editing, typesetting or other changes made by IOP Publishing and/or its licensors”

This Accepted Manuscript is © 2025 The Author(s). Published by IOP Publishing Ltd.



As the Version of Record of this article is going to be / has been published on a gold open access basis under a CC BY 4.0 licence, this Accepted Manuscript is available for reuse under a CC BY 4.0 licence immediately.

Everyone is permitted to use all or part of the original content in this article, provided that they adhere to all the terms of the licence <https://creativecommons.org/licenses/by/4.0>

Although reasonable endeavours have been taken to obtain all necessary permissions from third parties to include their copyrighted content within this article, their full citation and copyright line may not be present in this Accepted Manuscript version. Before using any content from this article, please refer to the Version of Record on IOPscience once published for full citation and copyright details, as permissions may be required. All third party content is fully copyright protected and is not published on a gold open access basis under a CC BY licence, unless that is specifically stated in the figure caption in the Version of Record.

View the [article online](#) for updates and enhancements.

Modeling of Graphene Wrapped Indium Antimonide Nanowire as thermo-optical Waveguide

Muhammad Sajid¹, Muhammad Zeshan Yaqoob^{2*}, Majeed A. S. Alkanhal³, Abdul Ghaffar⁴,
Ahtisham Ali⁵, Yasin Khan⁶

^{1,2} Department of Physics, Government College University, 38000, Faisalabad, Pakistan

^{3,6} Department of Electrical Engineering, King Saud University, Riyadh, Saudi Arabia

⁴ Department of Physics, University of Agriculture, Faisalabad, Pakistan

⁵ Department of Electronics and Telecommunications (DET), Politecnico di Torino, Torino, Italy

*Corresponding author: zeeshaan32@yahoo.com

Abstract

In this research work, the fiber modes supported by the graphene-wrapped indium antimonide nanowire have been examined theoretically. The indium antimonide (InSb) is a semiconductor material, which has temperature-sensitive optoelectronic properties. To model the nanowire of InSb, Drude's model has been used for better results. The Kubo's formalism based on the random phase approximation is used for the modeling of graphene. The impedance boundary conditions (IBCs) are used to compute the characteristic equations. The real and imaginary part of permittivity of InSb as function of THz frequency under different values of temperature $T \in [200 K, 400 K]$ has been computed. It is reported that the InSb shows the temperature dependent metal-insulator phase transition i.e., for temperature $T \leq 200K$ it behaves as insulator and for $T > 200K$ it acts as metal. The numerical results for dispersion relation, propagation band, propagation losses, cut off frequency range, effective mode index and field profiles have been presented for insulator as well as metallic phase of InSb. Moreover, the impact of chemical potential, radius, and temperature on fiber mode characteristics has been analyzed. The computed numerical results can be applied for designing tunable temperature assisted nano waveguides, thermo-optical sensing probes, thermal imaging and near-field communication devices in THz frequency range.

Key words: Terahertz, Graphene, Thermo-optical waveguide, Drude Model, Indium antimonide (InSb)

1-Introduction

Terahertz (THz) technology has emerged as a critical frontier in modern scientific research and applications, bridging the gap between microwave and infrared frequencies [1]. The unprecedented characteristics of THz radiation enable a wide range of applications including ultrafast wireless communication, biomedical imaging, and advanced sensing technologies [2, 3]. The study of the

1 THz waves has become a crucial element in research and development sector of the industries for
2 the manufacturing of the efficient THz devices for the ultra-fast transmission and next generation
3 imaging technologies, [4, 5]. The waveguides playing a crucial role in the development of next
4 generation THz technology by providing the active manipulation and control on the THz signals.
5 These structures play a crucial role in directing THz waves with minimal loss and distortion,
6 allowing for efficient transmission through different mediums. Several waveguide designs have
7 been created, such as metallic, dielectric, and photonic crystal waveguides, each tailored to
8 enhance the propagation properties of THz radiation. [6-9].

9 Graphene, an allotrope of the carbon with two dimensionality, is the one of the most promising
10 materials for THz waveguides due to its outstanding electrical and optical characteristics [10, 11].
11 Graphene integrated waveguide designs have unlocked new possibilities for THz applications,
12 enabling active tuning and improved signal manipulation. [12]. Studies have shown that graphene-
13 based plasmonic waveguides offer low loss and tunability, facilitating efficient signal transmission
14 at THz frequencies. [13, 14]. Moreover, researchers have investigated the combination of graphene
15 with different semiconductor materials to develop hybrid waveguide systems, offering enhanced
16 performance and new functionalities. [15, 16].

17 Many studies have been carried out regarding the graphene-based nanowires as waveguides i.e.,
18 Gao et al., developed the theoretical formulation for the plasmon supported by the graphene coated
19 dielectric nanowire (GNW) and discussed the characteristics of plasmon modes. They reported
20 that the properties of the plasmon modes can be tuned by varying the radius of the nanowire, the
21 dielectric permittivity, and the chemical potential of graphene [17]. To get the deeper physical
22 insights, Gao et al. conducted simulations of the plasmon waveguide modes supported by
23 graphene-coated nanowires (GNWs) using the finite element method (FEM) in COMSOL and they
24 computed the dispersion relation and propagation length, derived the number of supported modes
25 and the single-mode condition from an analytical model, and analyzed the characteristics of the
26 GNW by varying the graphene Fermi level [18]. To realize the reported work, the Chen et al.,
27 fabricated the graphene coated ZnO by using a tape-assisted transfer method under
28 micromanipulation. The enhanced strong surface optical feeds have been reported due to their
29 deep-subwavelength diameter and the high index contrast of the ZnO nanowires. They measured
30 the absorption of up to 0.11 dB/ μm in a 606-nm-diameter GZN at a wavelength of 1550 nm.
31 Furthermore, they observed the transmission modulation for a 1550-nm signal using a 590-nm-
32 diameter GZN, indicating the potential of GZN waveguides as nanoscale building blocks for
33 nanophotonic devices[19]. Gao et al. expanded upon this research by investigating the nonlinear
34
35
36
37
38
39
40
41
42
43
44
45
46
47
48
49
50
51
52
53
54
55
56
57
58
59
60

1 plasmonic coupling effects between closely spaced graphene-coated nanowires (GNWs). They
2 found that the routing of plasmons is sensitive to the input power delivered to the GNWs and is
3 influenced by the third-order conductivity of the graphene layer. Their findings provide insights
4 for designing tunable nanoplasmonic circuits using low-loss, edgeless cylindrical graphene
5 waveguides[20]. Yu, P. et al., investigated the detailed dispersion analysis of the graphene-coated
6 semiconductor nanowire and computed the proper and improper propagating modes in the
7 terahertz frequency range and classify them into trapped surface waves, fast and slow leaky waves,
8 and surface plasmons[21]. Golestanizadeh et al., carried out the theoretical investigations on the
9 acoustic plasmons supported by the semiconductor nanowire of indium antimonide (InSb) and its
10 dimmer under the frame work of hydrodynamic model. They have analyzed that the unlike metals,
11 semiconductors often require consideration of two or more types of plasma to accurately describe
12 their plasmonic behavior. A significant increase in the extinction cross-section and field
13 enhancement associated with acoustic localized surface plasmon resonance has been observed
14 [22]. Zhou et al., demonstrated the potential applications of the InSb nanowires for plasmonic
15 waveguides and real space imaging under external condition. This study performed a comparative
16 analysis of various materials—specifically Ag, graphene, hexagonal boron nitride (hBN), carbon
17 nanotubes (CNTs), tungsten diselenide (WSe₂), and InAs nanowires—in terms of their damping
18 ratios and confinement factors for plasmonic waveguiding applications. The results indicate that
19 InAs exhibits greater potential for tuning plasmonic waveguides, offering high confinement and
20 low propagation losses, making it a more favorable candidate compared to other noble metals and
21 2D materials[23].

22 This study aims to theoretically model graphene-wrapped InSb nanowires for use as thermo-
23 optical waveguides. InSb's optoelectronic properties, which are highly sensitive to temperature,
24 make it an attractive candidate for terahertz applications [24, 25]. The Graphene enables the active
25 tunability for the THz waves in the optoelectronic devices [26, 27]. To get the active control over
26 the propagation characteristics on the THz radiations, the use of graphene in for the InSb
27 waveguides has been motivated. Moreover, the Indium antimonide (InSb) is a temperature
28 sensitive material and shows the temperature assisted metal insulator transition [28, 29]. Therefore,
29 the theoretical study on the propagation characteristics of THz waves in the graphene coated InSb
30 nanowires under different temperature has been carried out. The present research work has been
31 conducted to achieve the following objectives i.e., (i) To compute the waveguide modes supported
32 by the graphene wrapped InSb nanowire for THz region, (ii) To analyze, how chemical potential,
33 frequency, and external temperature affect the propagation characteristics of waveguide modes
34
35
36
37
38
39
40
41
42
43
44
45
46
47
48
49
50
51
52
53
54
55
56
57
58
59
60

and (iii) To summarize the comparative analysis of waveguide modes in InSb, considering its roles as both an insulator and a conductor.

The manuscript is structured as follows: Section 2 presents the mathematical details of the analytical modeling of the warped graphene InSb nanowire as a waveguide, while Section 3 discusses the numerical results and their implications. Finally, the conclusions drawn from these findings are provided in the last section.

2. Analytical Formulations and Methodology

The mathematical modeling of the graphene-wrapped InSb nanowire as thermo-optical waveguide has been presented in this section. The waveguide is considered to be directed along the z-axis as depicted in the Fig.1. The propagation of the wave guided modes have been considered along the z-direction. The radius of the graphene wrapped InSb nanowire is considered as $r = a$. The region $r > a$ is considered as free space while the $r < a$ is taken as InSb nanowire and the graphene has been considered as negligible thickness at $r = a$ with a conductivity (σ_g). The conductivity of the graphene has been modeled in the frame work of semi-classical Kubo's formalism and expressed in terms of incident frequency (ω), temperature (T), chemical potential (μ_c), scattering rate (τ), Boltzmann constant (K_B) and reduced plank's constant (\hbar) as,

$$\sigma_g = i \frac{e^2 K_B T}{\pi \hbar^2 (\omega + \frac{i}{\tau})} \left(\frac{\mu_c}{K_B T} + 2 \ln \left[e^{-\frac{\mu_c}{K_B T}} + 1 \right] \right) + i \frac{e^2}{4\pi \hbar} \ln \left(\frac{2|\mu_c| - \hbar(\omega + \frac{i}{\tau})}{2|\mu_c| + \hbar(\omega + \frac{i}{\tau})} \right) \quad (1).$$

where the terms ω , μ , T , k_B , τ and \hbar stands for the incident frequency, chemical potential, temperature, Boltzmann constant, scattering rate and reduced plank's constant respectively [11-13]. This model assumes an idealized isotropic graphene layer, however the specific chirality configurations, such as zigzag and armchair edges, can influence the local electronic structure of graphene. To simplify the problem, the variation in the chirality configuration has not been added. For the structure considered in this study, the influence of armchair and zigzag chirality is minimal due to the wavelength of THz waves being much larger than the diameter of the nanowire. In this regime, the electromagnetic response of the graphene-wrapped InSb nanowire is predominantly governed by its macroscopic properties rather than the atomic-scale edge configurations. Consequently, the armchair and zigzag configurations are expected to behave similarly, with negligible differences in their impact on the propagation characteristics of the waveguide modes. The modeling of the indium antimonide (InSb) in the terahertz frequency range has been done by using the Drude model as follows [28, 29]:

$$\varepsilon_T = \varepsilon_\infty - \frac{\omega_p^2}{\omega^2 + i\gamma\omega} \quad (2)$$

where ε_∞ denotes high permittivity frequency, γ is damping constant, ω_p denotes plasma frequency with expression $\omega_p = \left(\frac{N(T)e^2}{\omega m^*}\right)^{\frac{1}{2}}$, where the m^* is effective mass of free charge carriers and “N(T)” is the temperature dependent charge carrier density and “e” represents the value of electronic charge.

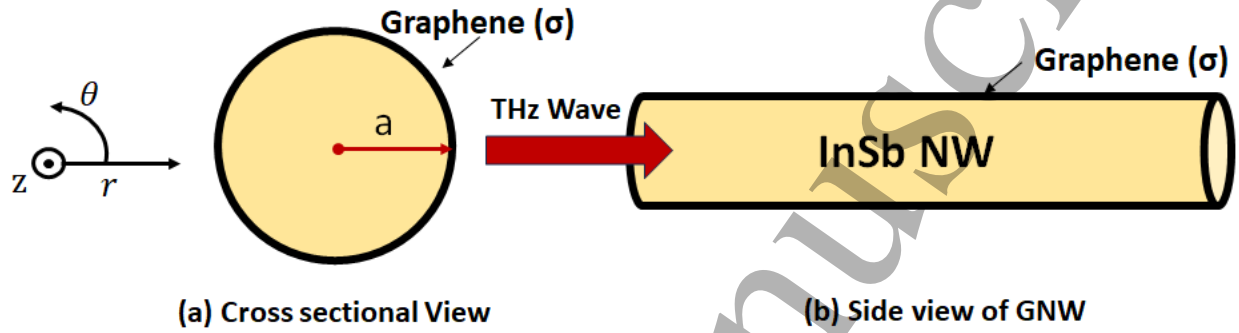


Figure.1: Schematic view of graphene wrapped InSb NW based thermo-optical waveguide

To solve the mathematical problem, the Maxwell's equations have been utilized to compute the wave equations with respect to each region. For the present work, the fundamental guided modes supported by graphene wrapped InSb NW based thermo-optical waveguide have been computed for the transverse magnetic (TM) polarization. The nanowire has been modeled as cylindrical shaped rod. To attain the symmetry in the mathematical equations, the waveguide modes has been formulated in the frame work of cylindrical coordinates (r, θ, z) . The guided modes in the frame work of the cylindrical coordinates are used to solve the equation satisfying \mathbf{E} and \mathbf{H} fields. An expression for the electric and magnetic field is be computed. In cylindrical coordinate (r, θ, z) an overall solution to the vector wave equation for source-free and lossless media by the wave equation as [17, 18]

$$(k^2 - \beta^2)E_r = i\beta \frac{\partial E_z}{\partial r} \quad (3)$$

$$(k_i^2 - \beta^2)H_\theta = i\omega\varepsilon_i \frac{\partial E_z}{\partial r} \quad (4)$$

Depending on whether $k_i^2 - \beta^2$ positive or negative, Fiber mode $k_2 < \beta < k_1$, Plasmon modes $\beta > k_1, k_2$

$$(k_i^2 - \beta^2)E_r = i\beta \frac{\partial E_z}{\partial r} \quad (5)$$

where the k_i corresponds to wavenumber of the respective region with $i=1, 2$. The solution of the above equations has been solved analytically to compute the electromagnetic modes in for the both regions i.e., inside the graphene-wrapped InSb NW ($r < a$) and

$$E_z = A J_0(\gamma_1 r) \quad (6)$$

$$E_r = \frac{i \beta A}{(k_1^2 - \beta^2)} \frac{\partial J_0(\gamma_1 r)}{\partial r} \quad (7)$$

$$H_\theta = \frac{i \omega \epsilon_T A}{(k_1^2 - \beta^2)} \frac{\partial J_0(\gamma_1 r)}{\partial r} \quad (8),$$

outside the graphene-wrapped InSb NW ($r > a$) as

$$E_z = B K_0(\gamma_2 r) \quad (9)$$

$$E_r = \frac{i \beta B}{(k_2^2 - \beta^2)} \frac{\partial K_0(\gamma_2 r)}{\partial r} \quad (10)$$

$$H_\theta = \frac{i \omega \epsilon_0 B}{(k_2^2 - \beta^2)} \frac{\partial K_0(\gamma_2 r)}{\partial r} \quad (11).$$

In the equations above, “A” and “B” represent the unknown coefficients corresponding to the fields in the regions $r < a$ and $r > a$ respectively. By applying the boundary conditions at the interface $r = a$, on the E & H fields as provided in [11, 12]

$$\left. \begin{aligned} E_z|^{+} &= E_z|^{-} \\ H_\theta|^{+} - H_\theta|^{-} &= E_z|^{-} \end{aligned} \right\} \quad (12)$$

The notations in the above boundary conditions stands for ‘+’ mean $r > a$ External and ‘-’ mean $r < a$ internal. By applying boundary conditions [12, 28]

$$\frac{\epsilon_T J_1(\gamma_1 a)}{\gamma_1 J_0(\gamma_1 a)} + \frac{\epsilon_0 K_1(\gamma_2 a)}{\gamma_2 K_0(\gamma_2 a)} = \frac{i \sigma_g}{\omega} \quad (13)$$

where the (J_1, J_0) and (K_1, K_0) stands for the Bessel functions and modified Bessel functions of first order and zero order respectively. The computed characteristics equation provides the mathematical solution of the wave guides modes by the graphene wrapped InSb nanowire. To get the physical insight, a detailed numerical solution has been presented in the subsequent section.

3. RESULTS AND DISCUSSION

The propagation characteristics of graphene based thermo-optical waveguide in the THz range have been presented in this section. In the first part, the temperature sensitive modeling of

the InSb nanowire in THz range has been presented in detail while in the second part, the propagation characteristics of waveguide modes have been discussed in detail.

3.1 EM Modeling of InSb nanowire as Temperature Sensitive Material

Figure 2 illustrates the real and imaginary components of the relative permittivity of InSb as a function of THz frequency, with variations in temperature. The permittivity of InSb is calculated using the Drude model, as described in Equation (2). The temperature dependent charge carrier density $N(T)$ is computed as $N = 5.76 \times 10^{20} T^{\frac{3}{2}} \exp(-\frac{E_g}{2k_B T})$, where E_g is the energy bandgap, T is temperature in Kelvin and k_B is the Boltzmann constant. The graphs for ϵ_r are presented for the temperature range of 200 K to 400 K. It is evident that the real part transitions from positive to negative as the temperature increases from 200 K to 360 K. This indicates that InSb behaves as an insulator at $T=200$ K, whereas for temperatures above 200 K, it exhibits conductive behavior. [25, 29].

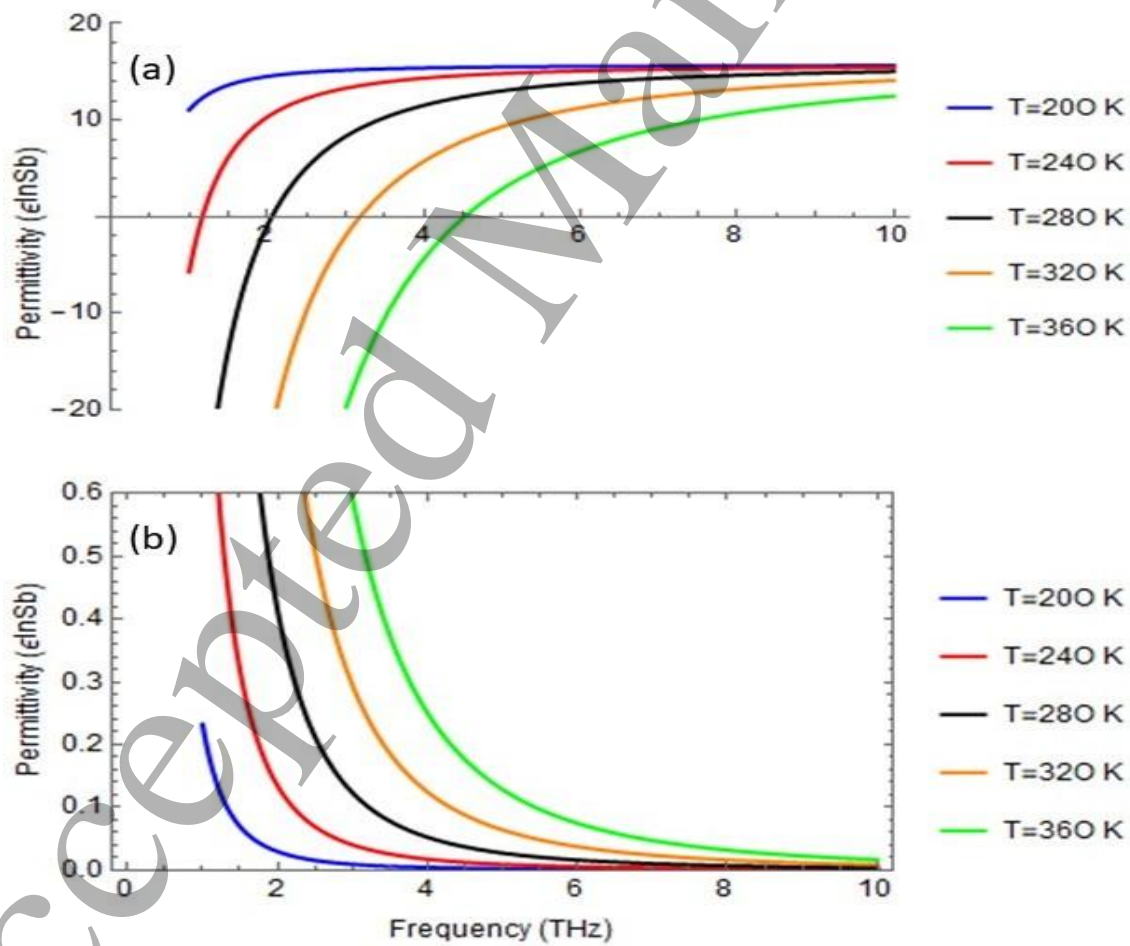


Figure 2: Modeling of the permittivity of InSb as a function of THz frequency: (a) Real part (b) Imaginary part with $\epsilon_{\infty}=15.68, \gamma = \pi * 10^{11} \text{ rad /s}$ & $E_g=0.26\text{eV}$.

3.2 Characteristics of thermo-optical waveguide

The fiber modes supported by the thermo-optical waveguide based on the graphene wrapped InSb nanowire have been computed. The characteristics equation (13) has been solved numerically in the frame work of the Wolfram Kernel in Mathematica software pack. To compute the roots of the characteristic equation, the contour plot technique has been implemented in the kernel. The propagation characteristics of the waveguide modes, propagation band, threshold frequency, propagation losses, damping effects, effective mode index and electric field profiles have been computed. Further the influence of temperature, radius of the waveguide and chemical potential of the graphene has been analyzed for all the computed results. To compute the propagation band and threshold frequency of waveguide modes supported by the graphene wrapped InSb nanowire, the dispersion curves in relation with frequency (f) and $Re(\beta)$ have been computed. Further, the influence of the temperature (T), chemical potential (μ_c) and radius of waveguide has been analyzed and presented in the Fig.3 to Fig5.

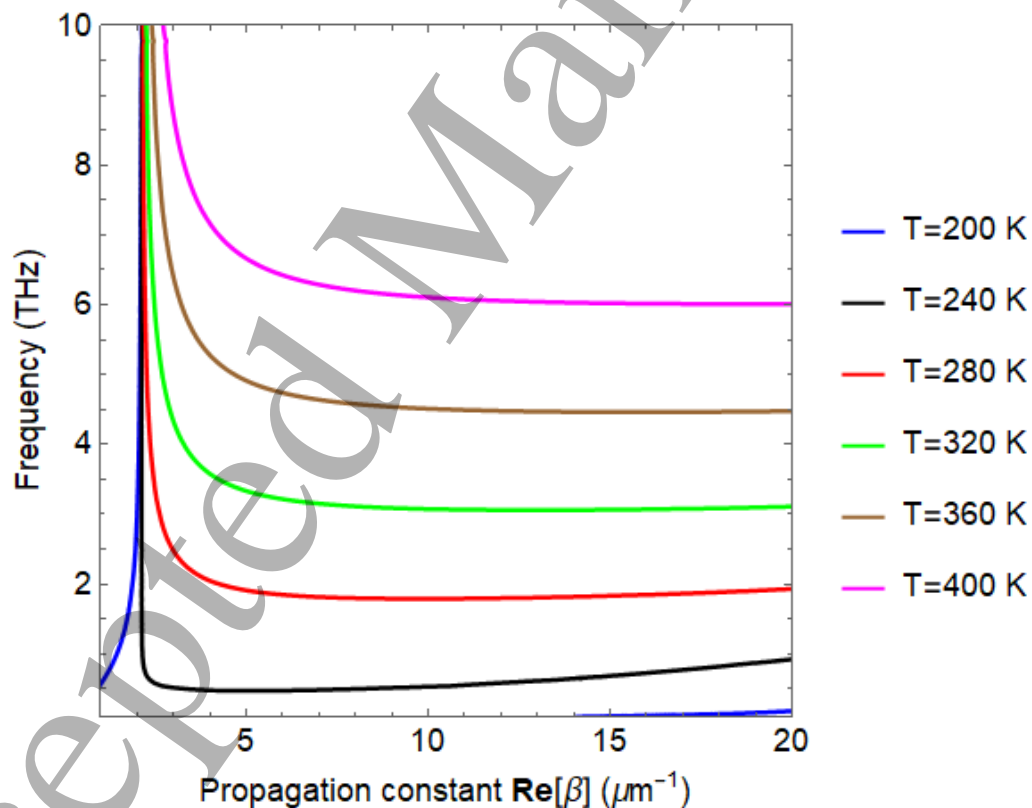
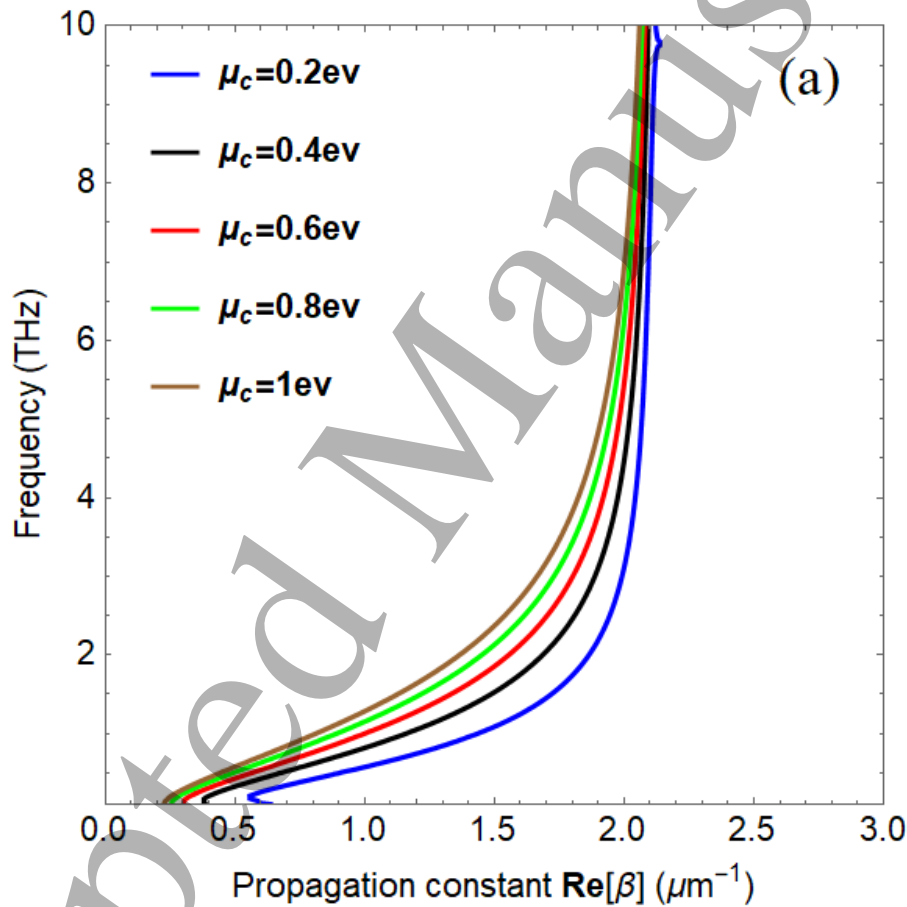


Figure 3: Dispersion Relation for various temperature at a constant radius of graphene wrapped InSb NW

The Fig.3 depicts the dispersion curve for the waveguide modes under the temperature variation $T \in [200, 240, 280, 320, 360, 400]K$. It is obvious from the Fig. that the with the increase of the

temperature, the propagation frequency and band gap increase. The possible reason for this trend is the increase of the plasma frequency (ω_p) of InSb with the increase of temperature. Further, it is important to note that the trend of the dispersion curve is same for the temperature 240 K to 400 K but for T=200K the trend is opposite. The major reason for such trend is temperature sensitive behavior of the InSb i.e., for the T=200 K, the InSb behave as insulator while for the T>200K it behaves as conductor, as explained in the Fig.2. To analyze the two distinct nature of waveguide modes viz., InSb as insulator (T=200K) and InSb as conductor (T=300K), the comparative analysis of the results has been shows in figure 4 and 5 for the different values of chemical potential and radius respectively.



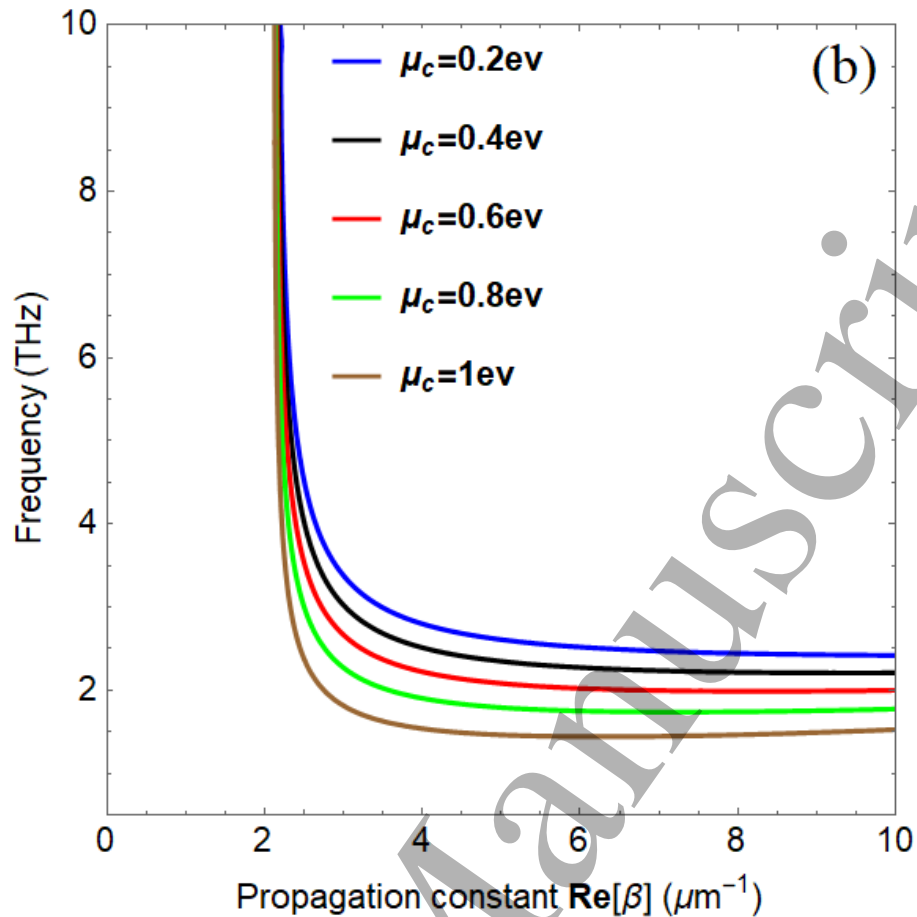


Figure 4: Dispersion relation for various values of chemical potential of graphene wrapped InSb NW (a) T=200K (b) T=300K

In Fig..4 the influence of the chemical potential (μ_c) on the propagation characteristics of the waveguide mode has been presented for the different values i.e., $\mu_c = 0.2eV, 0.4eV, 0.6eV, 0.8eV$ & $1.0 eV$. The Fig..4(a) delas with the waveguide modes supported by the graphene-wrapped InSb NW for T=200K while the Fig..4(b) presents the waveguide modes for T=300K. It can be analyzed that the modes are quite opposite to each other. The waveguide modes under T=200K, the graphene wrapped InSb as insulator, the propagation constant shifting towards the lower values with the increase of chemical potential and the speed of the propagating mode is increases with the increase of chemical potential. However, for the case of InSb as conductor at T=300K, the propagation frequency starts decreasing towards the lower THz with the increase of chemical potential (μ_c) and the speed of the propagating mode starts decreasing as provided in the Fig..4(b).

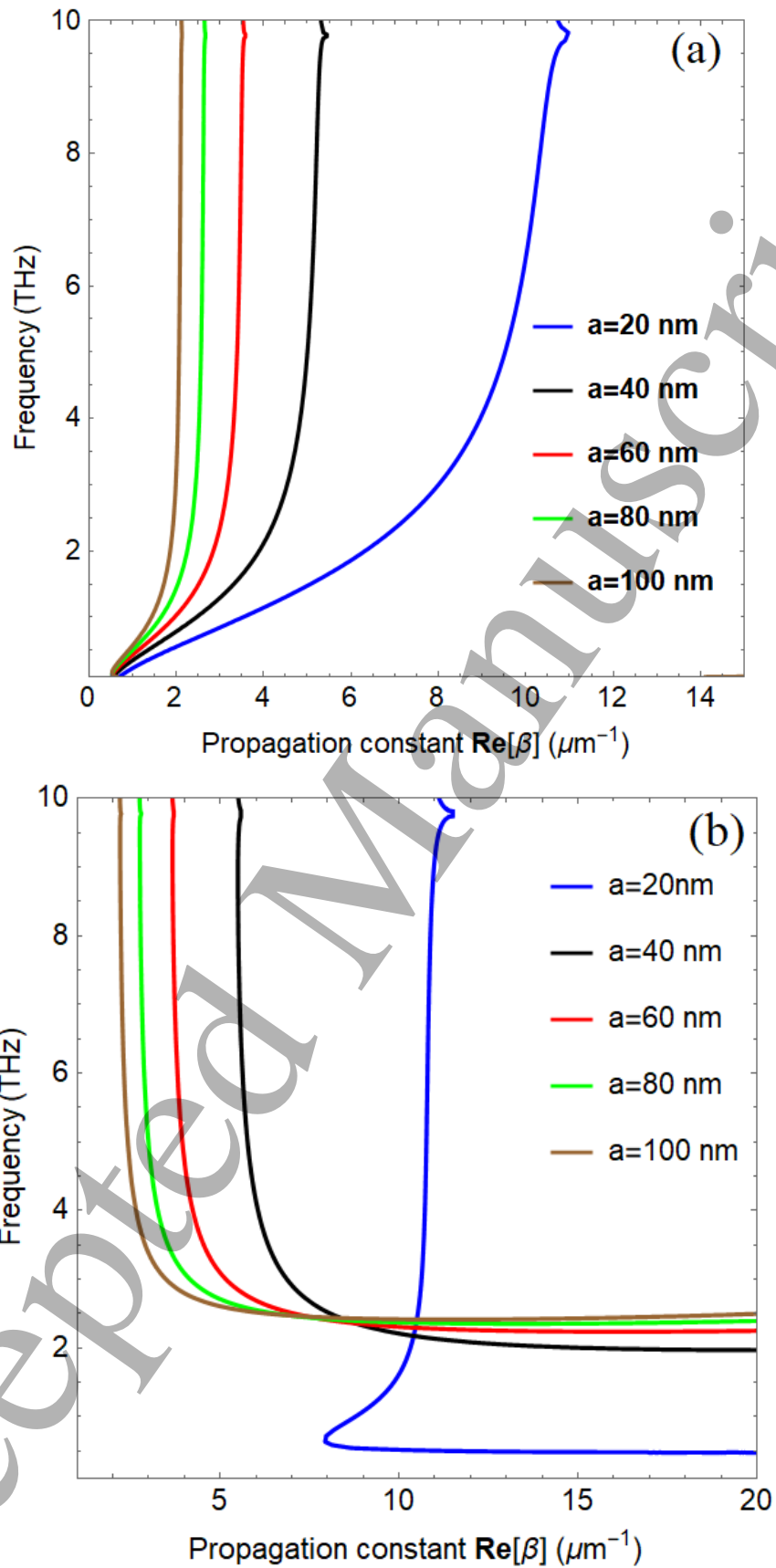


Figure 5 Dispersion relation for various values of diameter of graphene wrapped InSb NW (a)

T=200K (b) T=300K

The dimension of the waveguide plays important role in controlling the propagation frequency and cut off frequency. To analyze the propagation characteristics of the waveguide modes as function of structural parameters i.e., the dispersion curves have been plotted under different values of the radius of the graphene wrapped InSb thermo-optical waveguide i.e., $a = 20 \text{ nm}, 40 \text{ nm}, 60 \text{ nm}, 80 \text{ nm} \& 100 \text{ nm}$. The influence of the radius of the waveguide on the propagating modes under both configurations i.e., $T=200 \text{ K}$ and $T=300 \text{ K}$ has been presented in Fig. 5(a) and 5(b) respectively. For the case, graphene wrapped InSb nanowire at $T=200 \text{ K}$ in Fig. 5(a) that it is obvious from the Fig. that with the increase of the radius of waveguide, the propagation constant (β) shifting towards the lower value while the propagation frequency band ranges from 1 THz to 10 THz . For the case $T=300 \text{ K}$, it is clear from the Fig. 5(b) that at the radius $a=20 \text{ nm}$, the propagation mode has the lower cut off frequency while the cut off frequency shifting towards the high THz frequency range as the radius of the waveguide increases.

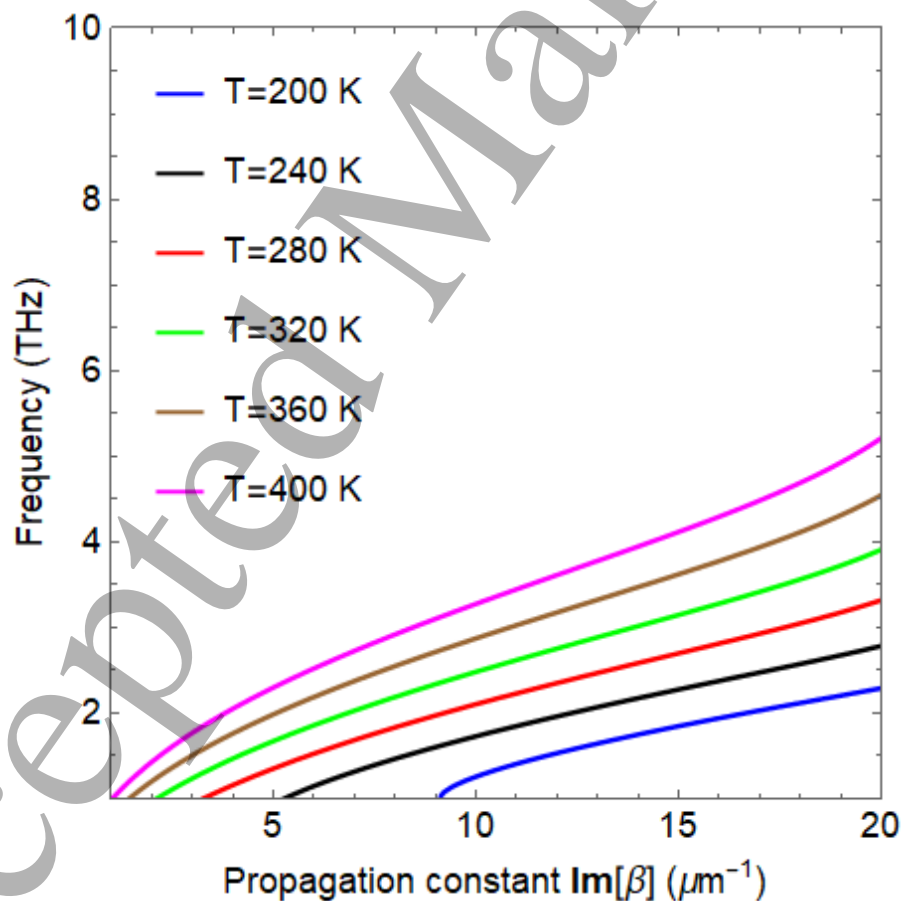


Figure 6: Propagation losses as a function of frequency for various temperatures of a graphene-wrapped InSb NW

1 To estimate the propagation losses and attenuation features of the graphene wrapped InSb
2 waveguide, numerical results between the operating frequency and $\text{Im}[\beta]$ have been plotted under
3 different values of the temperature i.e., $T \in [200, 240, 280, 320, 360, 400]K$. It can be concluded
4 that with the increase of temperature, the propagation losses and attenuation increase.
5
6

7
8 The figure 7 presents the impact of doping level of the graphene i.e., chemical potential (μ_c) on
9 the propagation losses of the waveguide modes under different temperature conditions i.e.,
10 $T=200K$ and $T=300 K$ Fig..7(a) and Fig..7(b) respectively. it is clear from the Fig. 7(a) that the
11 with the increase of chemical potential of the graphene, the losses have been increased significantly
12 as compared to the temperature variation and the second important trend is the propagation loss
13 corresponding to the high frequency values with the increase of chemical poetical (μ_c) as provided
14 in the other works[13, 15, 28]. However, for the case $T=300K$ when InSb behave as conducting
15 material, the propagation losses correspond to lower frequency values with the low damping
16 features as compared to the case when InSb behave as Insulator at $T=200K$. Further, it is depicted
17 in the Fig.7(b) that with the increase of chemical potential the propagation loss decreases as per
18 corresponding operating frequency. The figure 8 presents the radius dependent propagation loss
19 and damping features of the propagating mode under different values of radius i.e., $a =$
20 $20 \text{ nm}, 40\text{nm}, 60\text{nm}, 80 \text{ nm} \& 100\text{nm}..$ The Fig..8(a) provides the physical information about
21 the propagation loss and damping features of waveguide modes as function of operating frequency
22 for $T=200K$. It can be analyzed from figure that for this case, with the increase of radius of the
23 waveguide the variation in the propagation loss in indelible while for the case of $T=300K$ when
24 InSb behave as conductor, the propagation loss increases with the increase of the radius size from
25 $a=20 \text{ nm}$ to 100 nm . It is worth noting that the propagation frequency increases along with it.
26
27
28
29
30
31
32
33
34
35
36
37
38
39
40
41
42
43
44
45
46
47
48
49
50
51
52
53
54
55
56
57
58
59
60

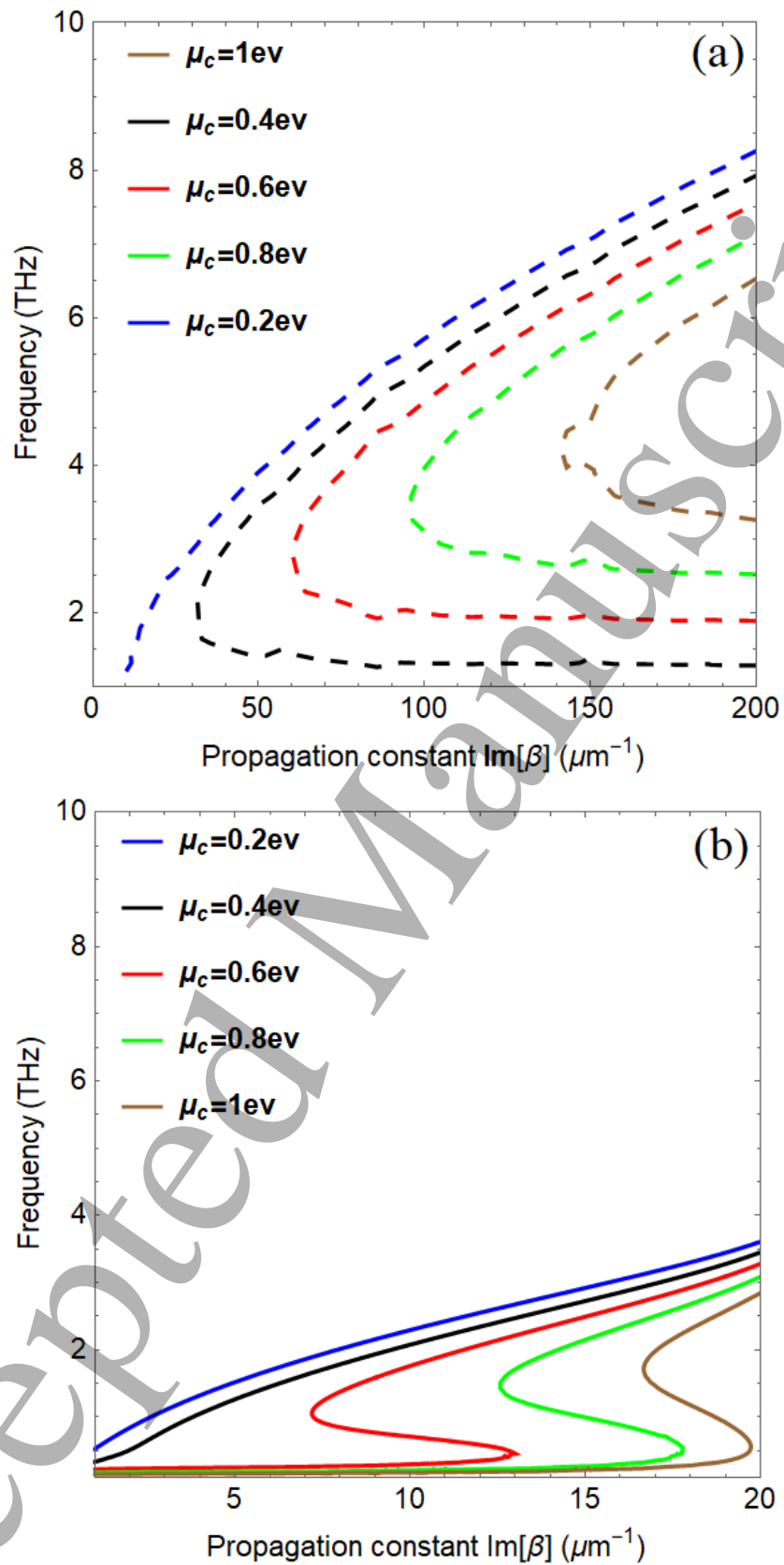


Figure 7: Propagation losses as a function of frequency for under different values of chemical potential of graphene for graphene wrapped InSb NW (a) $T=200\text{K}$ (b) $T=300\text{K}$

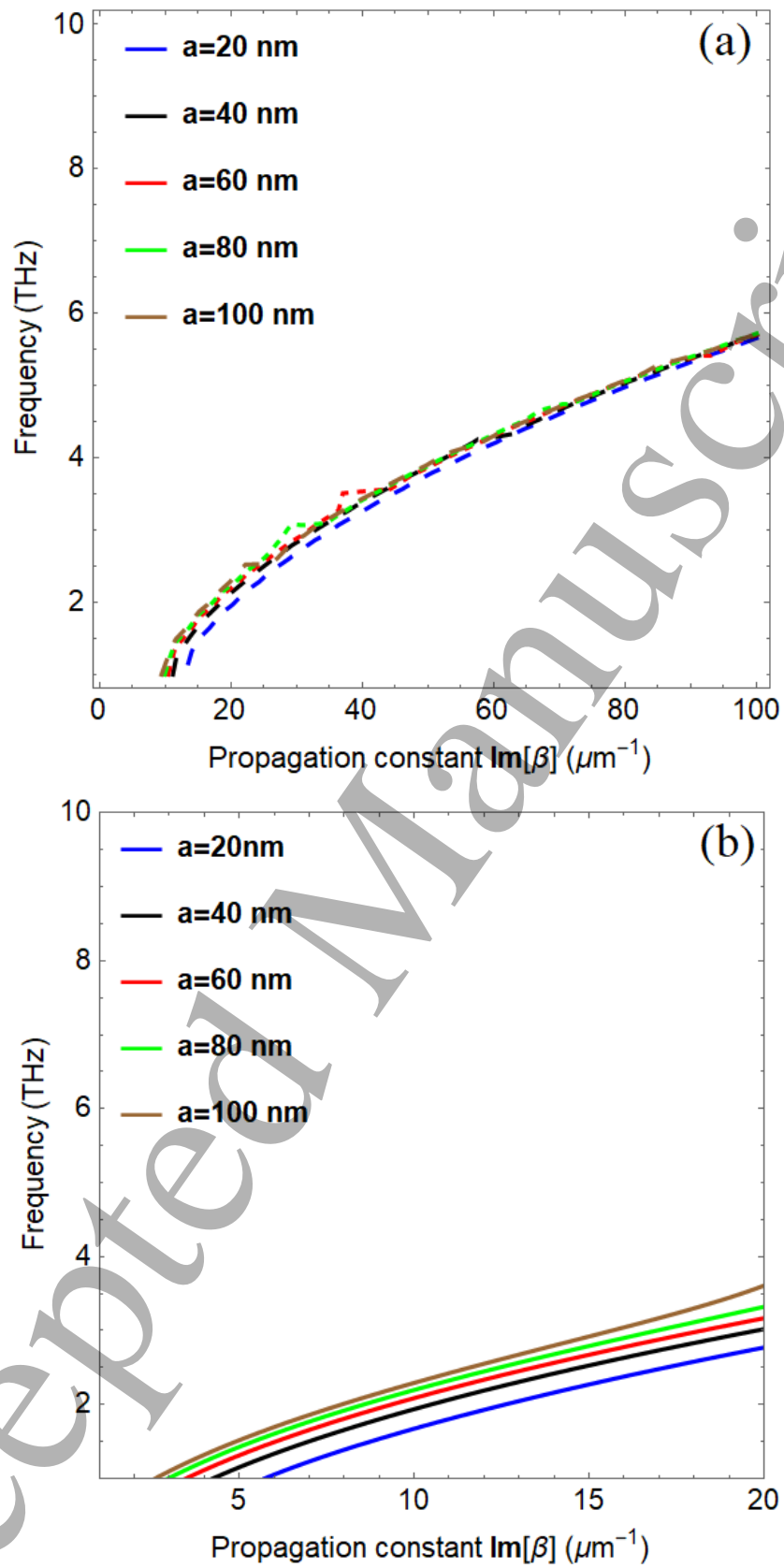


Figure 8: Propagation losses as a function of propagation frequency under different values of radius of graphene wrapped InSb NW based waveguide (a) $T=200\text{K}$ (b) $T=300\text{K}$

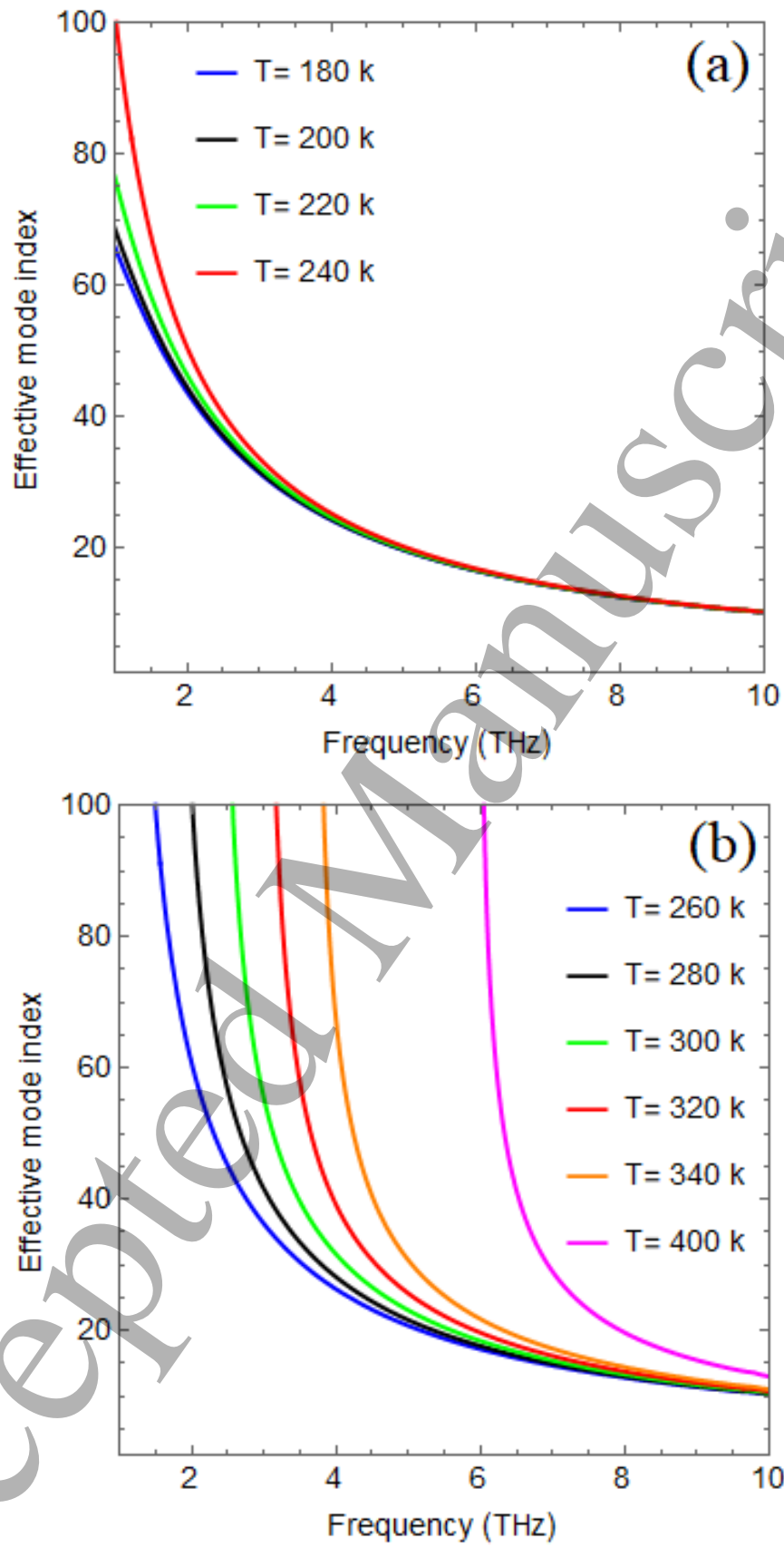


Figure 9: Effective mode index as function of frequency under different values of temperature

for graphene wrapped InSb NW based waveguide (a) InSb as insulator (b) InSb as conductor

The effective mode index is very important parameter for the designing and fabrication of the waveguides. It relates with the confinement of the propagating modes within the waveguide with respect to free wavevector (k_0) and its explicit mathematical expression is defined as $Re(\beta)/k_0$. The numerical results regarding the effective mode index as function of frequency under the variation of temperature (T), chemical potential (μ_c) and radius of waveguide (a) have been presented in Fig.9, 10, & 11 respectively. In Fig.9 it has shown that the effective mode index of the waveguide modes as function of the THz frequency under the temperature variation ($T \in [200, 400]K$) for two phases of the InSb i.e., Insulator phase and conductor phase. It can be deduced from the Fig.9(a) that under condition i.e., (InSb as insulator) the effective mode index of the waveguide modes monotonically decreases with the increase of the propagation frequency and for the frequency range (5 to 10) THz the effective mode index corresponds to constant value. Further it is clear that the effective mode index increases with the increase of temperature. In the scenario where InSb realized as a conductor, as illustrated in Figure 9(b), the effective mode index diminishes with increasing propagation frequency. Conversely, as the temperature rises, the propagation frequency begins to shift toward higher values, accompanied by a modest increase in the effective mode index.

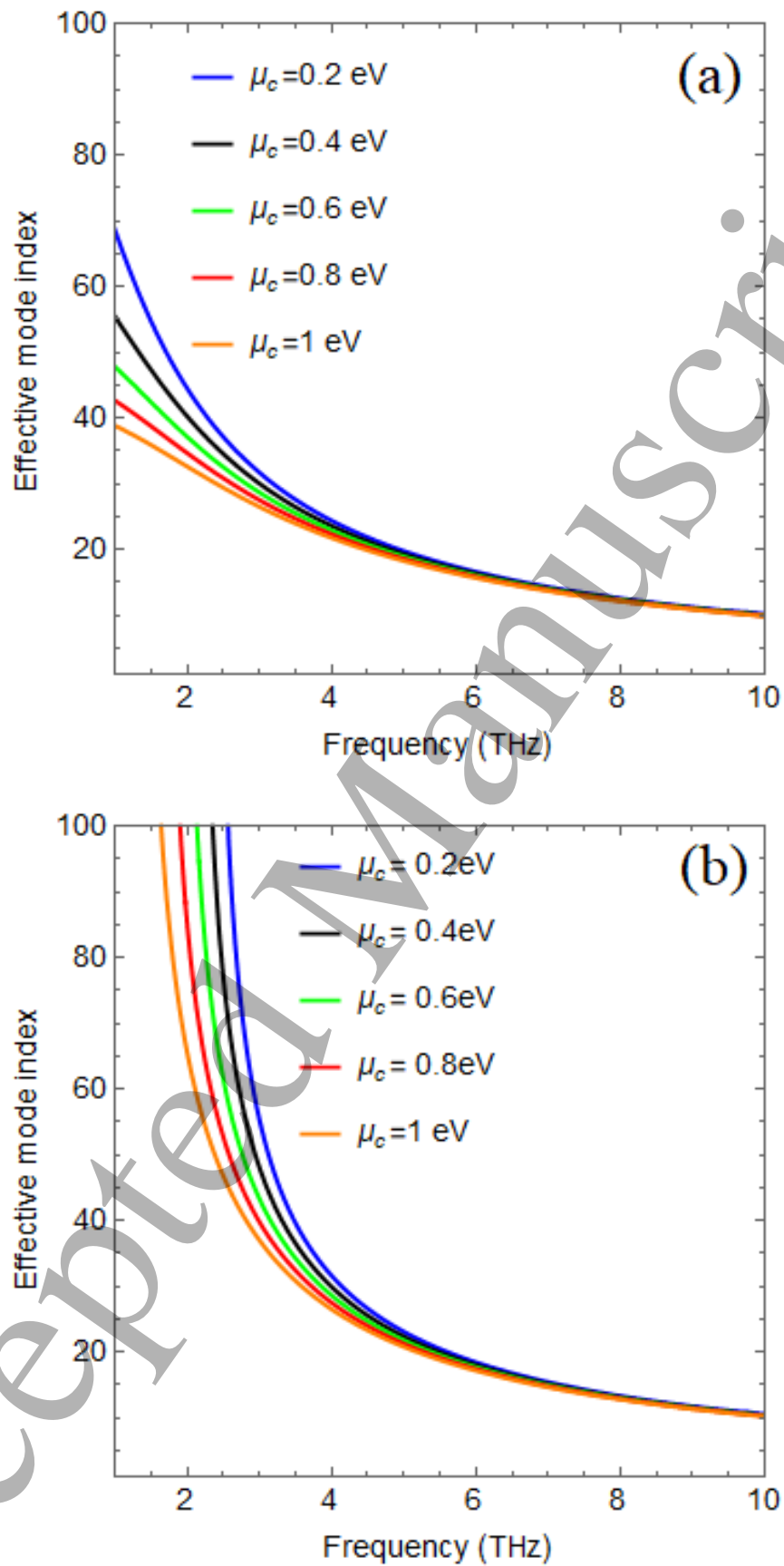
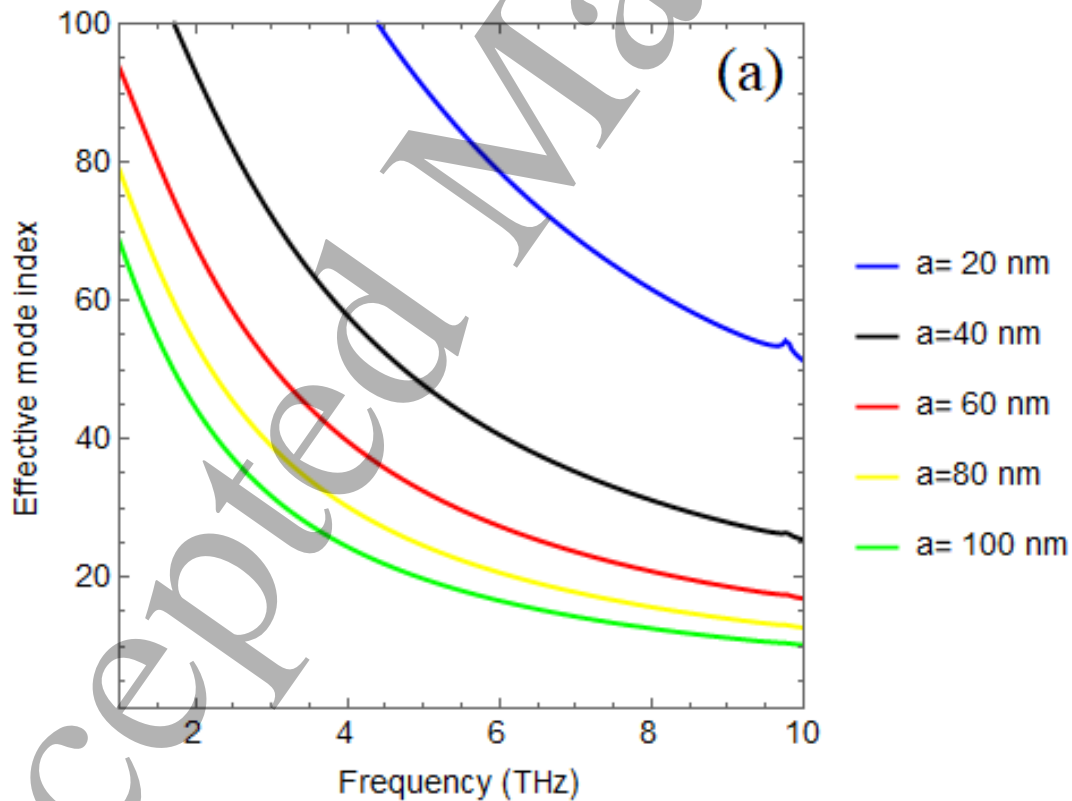


Figure 10: Effective mode index as function of frequency under different values of chemical

poetical for graphene wrapped InSb NW based waveguide (a) InSb as insulator $T=200\text{K}$ (b) InSb as conductor, $T=300\text{K}$

Figure 10 illustrates the effect of chemical potential on the effective mode index as a function of THz frequency for two states of InSb. The analysis examines various values of the chemical potential in the graphene waveguide, specifically within the range of $\mu_c \in (0.2 \text{ eV}, 0.4 \text{ eV}, 0.6 \text{ eV}, 0.8 \text{ eV}, \text{ and } 1.0 \text{ eV})$. In the case of $T = 200 \text{ K}$, where InSb acts as an insulator, the effective mode index decreases as the chemical potential rises. This reduction is attributed to increased losses associated with the elevated chemical potential of graphene, resulting in lower confinement of the waveguide modes in the graphene-wrapped InSb nanowire, as shown in Figure 10(a). In similar way, the figure 10(b) provides the analysis for impact of the chemical potential on the effective mode index for the case of $T = 300 \text{ K}$, where InSb acts as conductor. The figure clearly indicates that as the chemical potential increases, the effective mode index is associated with a reduced propagation band gap. Moreover, in relation to the propagation frequency, the effective mode index exhibits a decreasing trend.



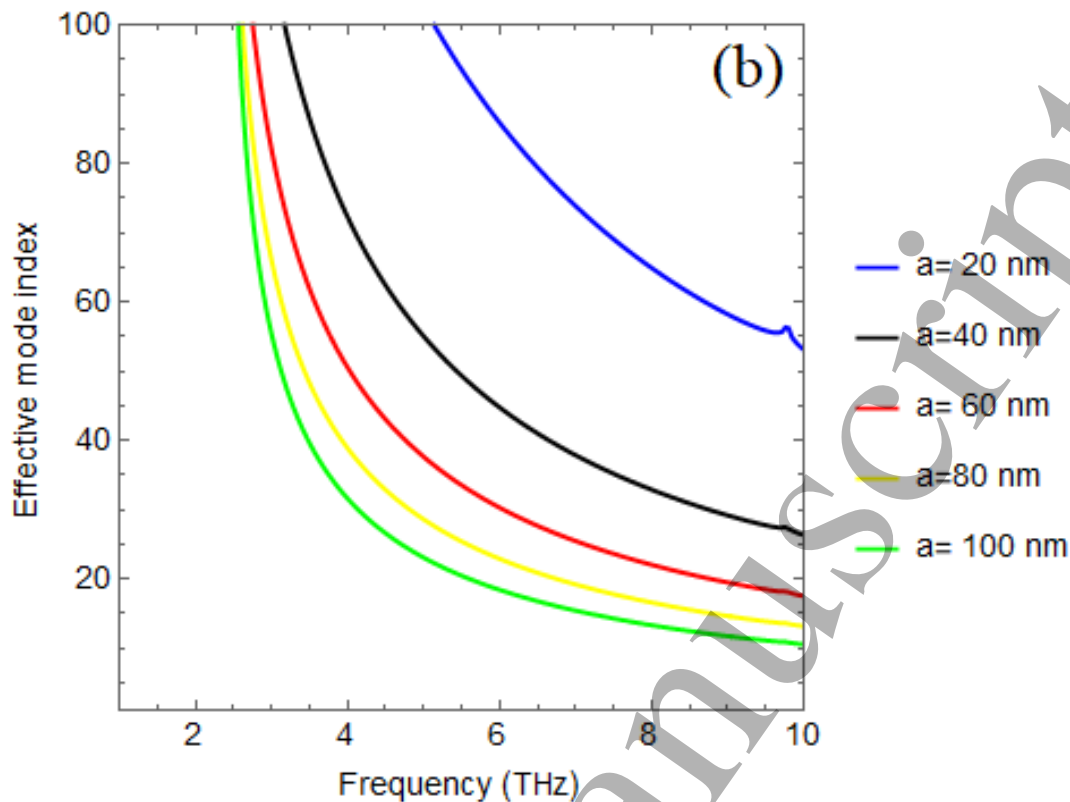
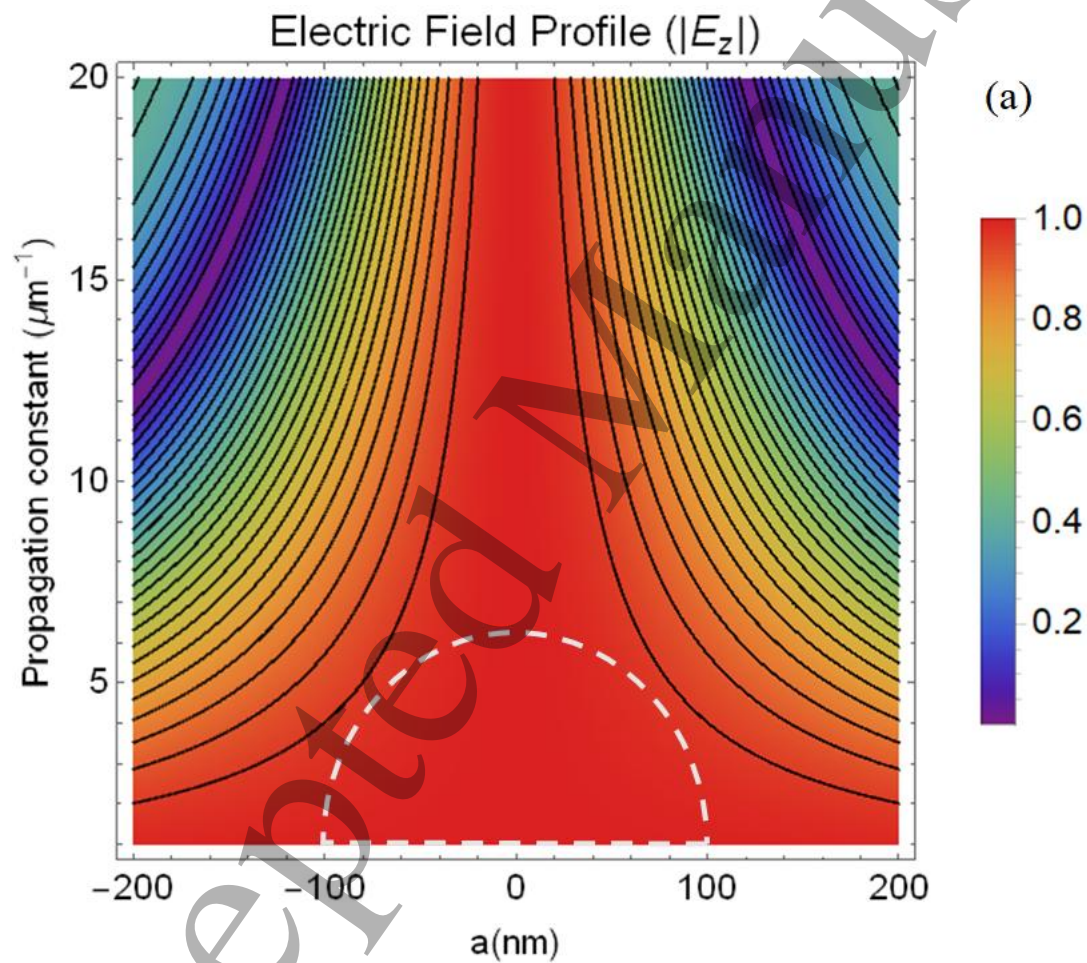


Figure 11: Effective mode index as function of frequency under different values of radius of graphene wrapped InSb NW based waveguide (a) InSb as insulator $T=200\text{K}$ (b) InSb as conductor, $T=300\text{K}$

To analyze the dimensional impact on the confinement of the waveguide modes of the graphene wrapped InSb nanowire, the effective mode index has been computed under different values of radius of waveguide i.e., $a = 20\text{ nm}$, 40 nm , 60 nm , 80 nm & 100 nm in figure 11. The effective mode index has been presented for InSb as insulator and conductor in fig11(a) and Fig. 11(b) respectively. These figures clearly demonstrate that as the waveguide radius increases, the effective mode index decreases. This trend is further associated with the cutoff frequency of the waveguide, indicating an inverse relationship between waveguide size and propagation frequency. It is worth mentioning that the relationship between the diameter of InSb nanowires and their corresponding bandgap energies has been carefully considered. It is well-documented that quantum confinement effects significantly influence the bandgap energy as the diameter decreases below a critical threshold [30]. For diameters larger than 65 nm , the bandgap energy remains nearly identical to that of the bulk material (0.17 eV) due to negligible confinement effects. However, as the diameter reduces from 65 nm to 30 nm , a modest increase in bandgap energy is observed, ranging from 0.17 eV to 0.20 eV . A more pronounced increase occurs when the diameter decreases

1 further, from 30 nm to 5 nm, with the bandgap energy rising sharply from 0.20 eV to 1.2 eV. These
2 changes in bandgap energy are particularly relevant in the mid-infrared (MWIR) and near-infrared
3 (NIR) regions, enabling InSb nanowires to support multi-spectrum detection. For diameters
4 exceeding 10 nm, the bandgap energies are aligned with MWIR detection, while smaller diameters
5 extend this capability to the NIR region[30, 31]. However, the current study is focused on the THz
6 frequency range, where the optical properties of InSb nanowires are primarily dictated by a
7 temperature-driven phase transition from an insulating to a metallic state. In this regime, variations
8 in bandgap energy due to diameter changes are negligible compared to the dominant thermal
9 effects influencing the optical response. Consequently, size-dependent optical variations are not
10 significant for the parameters under investigation.



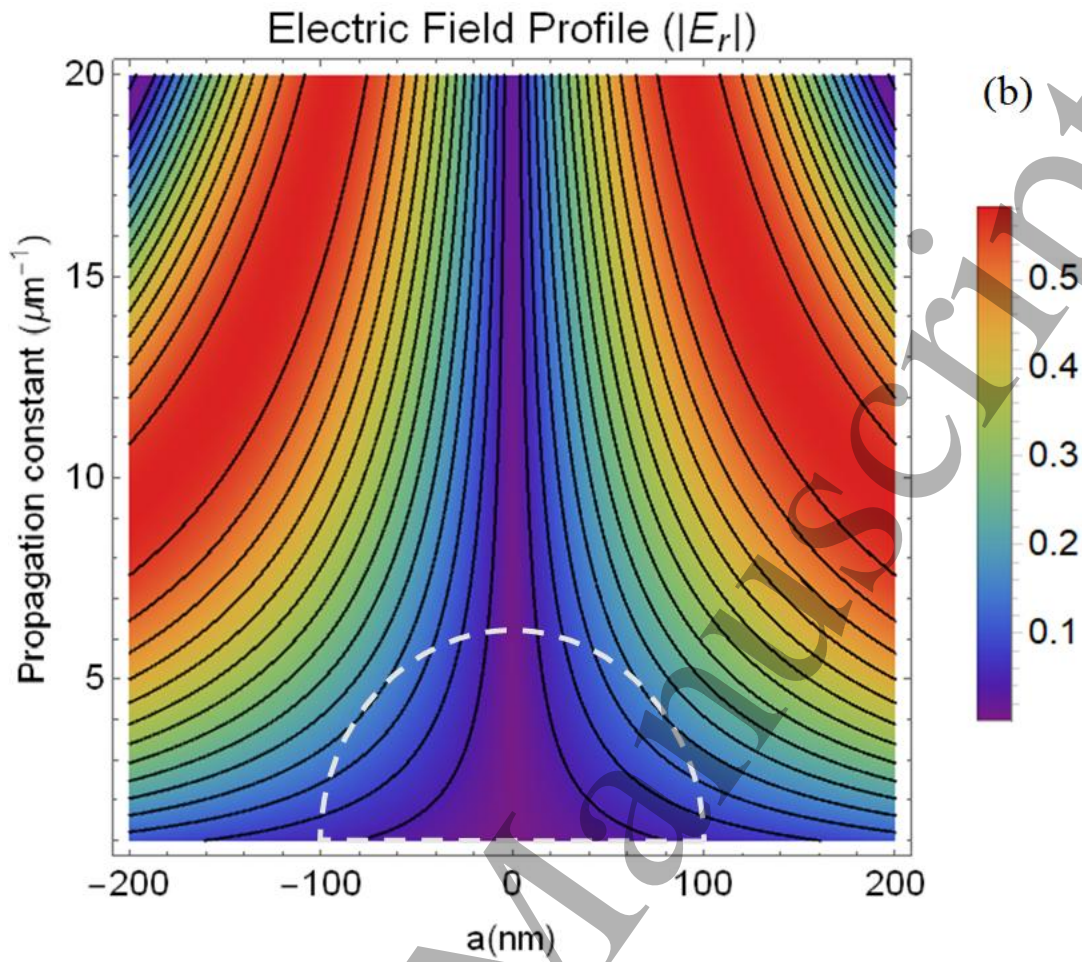


Figure 12: Normalized electric field profiles for the graphene-wrapped InSb NW with 100nm radius (a) $|E_z|$ and (b) $|E_r|$ at $f = 1 \text{ THz}$, $T = 300 \text{ K}$ & $\mu_c = 0.2 \text{ eV}$

In the figure 12, the density plots for the electric field profiles ($|E_z|$ & $|E_r|$) as a function of radial distance (a) and the propagation constant (β) for the graphene-wrapped InSb nanowire waveguide at THz frequencies is presented. The dotted semi-circle in the figs represents cross-sectional view of the NW. From fig.12(a), it can be deduced that the electric field profile is symmetric about the center of the nanowire, indicating a uniform distribution influenced by the cylindrical geometry of the nanowire. It can be analyzed that the field strength $|E_z|$ is maximum at the center and decreases smoothly toward the edges i.e., $a = \pm 100 \text{ nm}$. This behavior is typical for the fundamental mode in waveguides, where the field is strongest at the core and diminishes in the surrounding medium due to boundary conditions and waveguide confinement. The confinement arises from the unique optical properties of graphene, which include its high conductivity and ability to sustain plasmonic modes at THz frequencies[32]. This allows for effective localization of the electromagnetic field even when the wavelength is much larger than the nanowire dimensions. The strong dependence

of the field distributions on the propagation constant (β) is evident in the results. Larger values of β are associated with enhanced confinement of the field within the nanowire core. This is a direct result of the proportionality between β and the effective mode index, which increases with greater field localization. The radial component of the electric field ($|E_r|$) for the waveguide is depicted in Fig. 12(b). It is evident that the radial electric field is minimal at the center of the waveguide and reaches its maximum at the edges. This suggests that the radial component of the electric field is weakly confined at the core of the waveguide. As the radius increases, the magnitude of $|E_r|$ grows, reaching a maximum at the waveguide boundaries. Further, it can be inferred from the tightly packed contours at the higher propagation constant ($\beta > 15 \mu\text{m}^{-1}$), the field is highly confined as compared to the lower values of propagation constant ($\beta < 10 \mu\text{m}^{-1}$). The contours get wider for lower value, depicting the less confinement. The strong radial electric field near the boundaries could be utilized in sensing or surface-enhanced applications, as the field interacts more significantly with the surrounding environment. Moreover, the careful selection of field distributions and propagation constants can be employed to optimize and design thermo-optical waveguides. As provided in the figures 9-11 that the effective mode index can be tuned by tailoring the external frequency, temperature and radius of NW, the impact of these parameters under the variation of frequency and corresponding effective mode index has been presented in the fig.13.

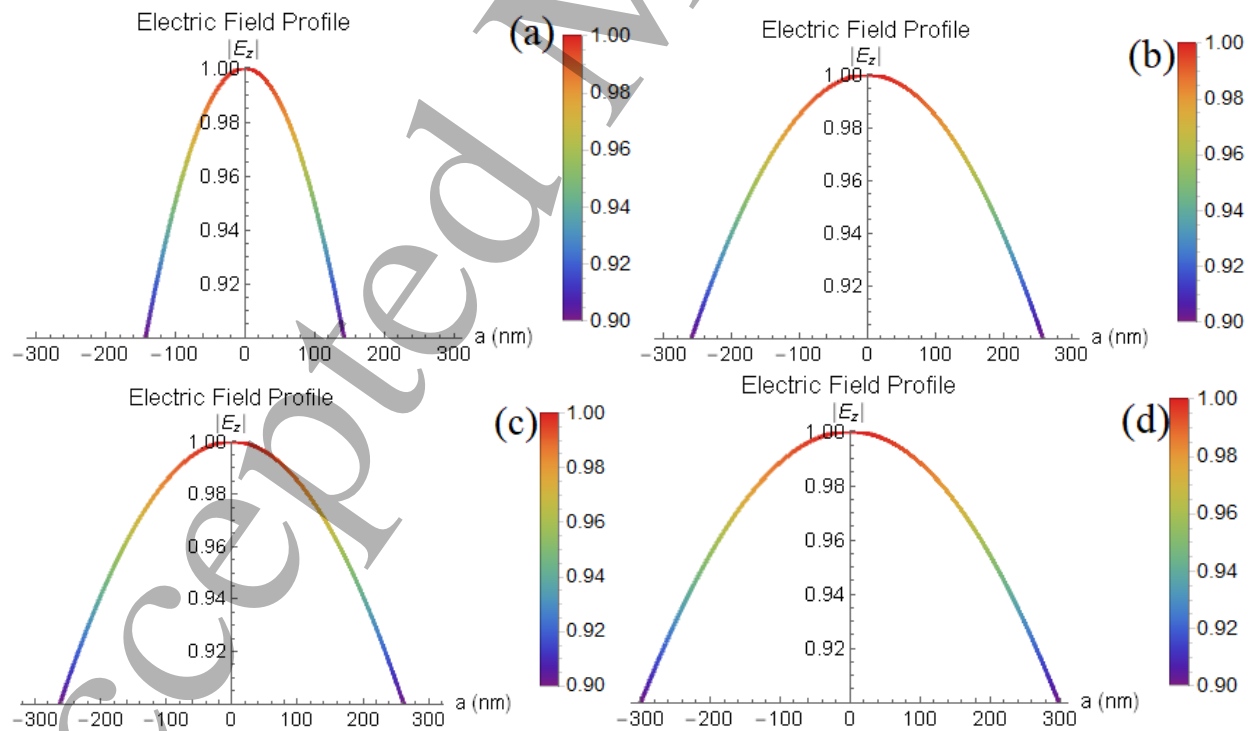


Fig.13 Spatial Field distribution inside and outside of graphene wrapped NW of radius 100 nm (a) At $f = 2.63\text{THz}$, $N_{\text{eff}}=81.31$ (b) At $f = 4.54\text{THz}$, $N_{\text{eff}}=26.24$ (c) At $f = 6.57\text{THz}$, $N_{\text{eff}}=16.41$ (d) At $f = 8.95\text{THz}$, $N_{\text{eff}}=11.49$

The results illustrated in Fig. 13 pertain to the behavior of modes both within and outside the waveguide. These findings were derived by examining the electric field distribution as a function of the waveguide radius across different frequencies, alongside their corresponding effective mode indices (N_{eff}). It can be inferred from these results that as the effective mode index increases the field profile expanded and transformed into the leaky type modes. It is obvious from the fig.13(a), at the lower frequency ($f=2.63\text{ THz}$, $N_{\text{eff}}=81.31$), the effective mode index is much higher, indicating strong confinement of the modes within the waveguide. This is reflected in the highly localized electric field profile near the waveguide surface. As the frequency increases ($f=4.54\text{ THz}$, $N_{\text{eff}}=26.24$), ($f=4.54\text{ THz}$, $N_{\text{eff}}=26.24$) & ($f=4.54\text{ THz}$, $N_{\text{eff}}=26.24$) the effective mode index decreases. This reduction corresponds to weaker confinement of the modes, with the electric field spreading further away from the waveguide surface as give in fig 13(b), (c) and (d) respectively. Additionally, to understand the effect of temperature on the field profiles, Fig. 9 shows that as the temperature increases, the effective mode index also increases. This suggests that higher temperatures lead to stronger confinement of the waveguide modes compared to lower temperatures. The computed results highlight a gradual decrease in N_{eff} with increasing frequency, indicating a transition in the characteristics of the guided modes. The fields extend farther from the surface, suggesting that the modes become less confined within the waveguide structure.

4. Concluding Remarks

This study presents a comprehensive analysis of the fiber modes supported by thermo-optical waveguides utilizing graphene-wrapped InSb nanowires. Using numerical solutions of the characteristic equation through Mathematica, we analyzed the propagation characteristics of graphene-wrapped InSb nanowires, focusing on the effective mode index, propagation band, threshold frequency, and propagation losses under varying temperature, waveguide radius, and chemical potential conditions. The findings indicate a notable temperature dependence, with InSb shifting from an insulating state at 200 K to a conducting state at higher temperatures. This transition significantly impacts the propagation characteristics, demonstrated by contrasting trends in propagation constants and damping features at different temperatures. Additionally, our analysis shows that increasing the chemical potential of graphene produces varied effects on the propagation characteristics, emphasizing the distinct behaviors of waveguide modes in both

insulating and conducting states. The effects of waveguide dimensions were also examined, revealing that larger waveguide radii lead to a decrease in the effective mode index and shifts in cutoff frequency. This relationship highlights the importance of structural parameters in optimizing waveguide performance. Ultimately, this research improves our understanding of the intricate interactions between temperature, chemical potential, and structural dimensions in graphene-wrapped InSb nanowire waveguides, offering valuable insights for future photonic device applications.

Authors' Contributions: M. Sajid and M. Z. Yaqoob wrote main manuscript and derived analytical expressions. Majeed A. S. Alkanhal and Abdul Ghaffar edited the manuscript and reviewed the numerical analysis., Ahtisham Ali and Yasin developed methodology and analysis of results and discussion in the given study. All authors reviewed the manuscript before submission.

Availability of Data and Materials: Detail about data has been provided in the article.

Acknowledgments: This work was supported by the Researchers Supporting Project number (RSPD2024R985), King Saud University, Riyadh, Saudi Arabia.

References

1. Pang, X., O. Ozolins, S. Jia, L. Zhang, R. Schatz, A. Udalcovs, V. Bobrovs, H. Hu, T. Morioka, and Y.-T. Sun, *Bridging the terahertz gap: Photonics-assisted free-space communications from the submillimeter-wave to the mid-infrared*. Journal of Lightwave Technology, 2022. **40**(10): p. 3149-3162.
2. Shen, S., X. Liu, Y. Shen, J. Qu, E. Pickwell-MacPherson, X. Wei, and Y. Sun, *Recent advances in the development of materials for terahertz metamaterial sensing*. Advanced Optical Materials, 2022. **10**(1): p. 2101008.
3. Gong, A., Y. Qiu, X. Chen, Z. Zhao, L. Xia, and Y. Shao, *Biomedical applications of terahertz technology*. Applied Spectroscopy Reviews, 2020. **55**(5): p. 418-438.
4. Akyildiz, I.F., J.M. Jornet, and C. Han, *Terahertz band: Next frontier for wireless communications*. Physical communication, 2014. **12**: p. 16-32.
5. Song, H.-J. and N. Lee, *Terahertz communications: Challenges in the next decade*. IEEE Transactions on Terahertz Science Technology, 2021. **12**(2): p. 105-117.
6. Carnio, B.N., O. Moutanabbir, and A.Y. Elezzabi, *Nonlinear photonic waveguides: A versatile platform for terahertz radiation generation (a review)*. Laser Photonics Reviews, 2023. **17**(4): p. 2200138.
7. Shi, L.-F., A. Zahid, A. Ren, M.Z. Ali, H. Yue, M.A. Imran, Y. Shi, and Q.H. Abbasi, *The perspectives and trends of THz technology in material research for future communication-a comprehensive review*. Physica Scripta, 2023. **98**(6): p. 065006.
8. Tan, Z., Q.Y. Zhang, Y.L. Lei, Y. Zhao, and J.Q. Ding, *Terahertz waveguide multiplexers: A review*. Microwave Optical Technology Letters, 2023. **65**(7): p. 1925-1935.
9. Katyba, G., K. Zaytsev, I. Dolganova, N. Chernomyrdin, V. Ulitko, S. Rossolenko, I. Shikunova, and V. Kurlov, *Sapphire waveguides and fibers for terahertz applications*. Progress in Crystal Growth Characterization of Materials, 2021. **67**(3): p. 100523.

10. Guo, T. and C. Argyropoulos, *Recent advances in terahertz photonic technologies based on graphene and their applications*. Advanced Photonics Research, 2021. **2**(6): p. 2000168.
11. Depine, R.A., *Graphene optics: electromagnetic solution of canonical problems*. 2016: Morgan & Claypool Publishers.
12. Saeed, M., A. Ghaffar, S.U. Rehman, M.Y. Naz, S. Shukrullah, and Q.A. Naqvi, *Graphene-based plasmonic waveguides: a mini review*. Plasmonics, 2022. **17**(3): p. 901-911.
13. Ye, L., K. Sui, Y. Liu, M. Zhang, and Q.H. Liu, *Graphene-based hybrid plasmonic waveguide for highly efficient broadband mid-infrared propagation and modulation*. Optics express, 2018. **26**(12): p. 15935-15947.
14. Zheng, K., Y. Yuan, L. Zhao, Y. Chen, F. Zhang, J. Song, and J. Qu, *Ultra-compact, low-loss terahertz waveguide based on graphene plasmonic technology*. 2D Materials, 2019. **7**(1): p. 015016.
15. Kim, J.T., J.-H. Choe, J.-S. Kim, D. Seo, Y.D. Kim, and K.H. Chung, *Graphene-based plasmonic waveguide devices for electronic-photonics integrated circuit*. Optics Laser Technology, 2018. **106**: p. 76-86.
16. Zhang, Y., J. Wu, L. Jia, Y. Qu, Y. Yang, B. Jia, and D.J. Moss, *Graphene oxide for nonlinear integrated photonics*. Laser Photonics Reviews, 2023. **17**(3): p. 2200512.
17. Gao, Y., G. Ren, B. Zhu, H. Liu, Y. Lian, and S. Jian, *Analytical model for plasmon modes in graphene-coated nanowire*. Optics express, 2014. **22**(20): p. 24322-24331.
18. Gao, Y., G. Ren, B. Zhu, J. Wang, and S. Jian, *Single-mode graphene-coated nanowire plasmonic waveguide*. Optics letters, 2014. **39**(20): p. 5909-5912.
19. Chen, B., C. Meng, Z. Yang, W. Li, S. Lin, T. Gu, X. Guo, D. Wang, S. Yu, and C.W. Wong, *Graphene coated ZnO nanowire optical waveguides*. Optics Express, 2014. **22**(20): p. 24276-24285.
20. Gao, Y. and I.V. Shadrivov, *Nonlinear coupling in graphene-coated nanowires*. Scientific Reports, 2016. **6**(1): p. 38924.
21. Yu, P., V.I. Fesenko, and V.R. Tuz, *Dispersion features of complex waves in a graphene-coated semiconductor nanowire*. Nanophotonics, 2018. **7**(5): p. 925-934.
22. Golestanizadeh, T., A. Zarifi, T. Jalali, J.R. Maack, and M. Wubs, *Hydrodynamic acoustic plasmon resonances in semiconductor nanowires and their dimers*. JOSA B, 2019. **36**(10): p. 2712-2720.
23. Zhou, Y., R. Chen, J. Wang, Y. Huang, M. Li, Y. Xing, J. Duan, J. Chen, J.D. Farrell, and H. Xu, *Tunable low loss 1D surface plasmons in InAs nanowires*. Advanced Materials, 2018. **30**(35): p. 1802551.
24. Zhang, C., Y. Liu, J. Li, Q. Wu, and M. Li, *Design of a highly sensitive terahertz temperature and refractive index composite sensor based on an InSb–Ag composite grating*. JOSA B, 2024. **41**(2): p. 411-420.
25. Yaqoob, M., M. Ahamd, A. Ghaffar, F. Razzaz, S. Saeed, and T. Alanazi, *Thermally tunable electromagnetic surface waves supported by graphene loaded indium antimonide (InSb) interface*. Scientific Reports, 2023. **13**(1): p. 18631.
26. Zhou, Q., Q. Qiu, and Z. Huang, *Graphene-based terahertz optoelectronics*. Optics Laser Technology, 2023. **157**: p. 108558.
27. Chen, X., Z. Tian, Q. Li, S. Li, X. Zhang, C. Ouyang, J. Gu, J. Han, and W. Zhang, *Recent progress in graphene terahertz modulators*. Chinese Physics B, 2020. **29**(7): p. 077803.

- 1 28. Yaqoob, M., M. Anwar, A. Ghaffar, M.A. Alkanhal, Y. Khan, and M. Shahid,
2 *Temperature-assisted electromagnetic surface modes in graphene-based temperature*
3 *sensitive metafilms*. Optics Continuum, 2024. **3**(5): p. 714-731.
- 4 29. Zainud-Deen, S.H., H.A.E.-A. Malhat, and E.A.A. El-Refaay, *InSb based microstrip*
5 *patch antenna temperature sensor for terahertz applications*. Wireless Personal
6 Communications, 2020. **115**(1): p. 893-908.
- 7 30. Chen, H., K.W.C. Lai, X. Sun, N. Xi, and M. Meyyappan, *Indium antimonide (InSb)*
8 *nanowire-based photodetectors*, in *Nano Optoelectronic Sensors and Devices*. 2012,
9 Elsevier. p. 209-224.
- 10 31. Xu, T., H. Wang, X. Chen, M. Luo, L. Zhang, Y. Wang, F. Chen, C. Shan, and C.J.N.
11 Yu, *Recent progress on infrared photodetectors based on InAs and InAsSb nanowires*.
12 Nanotechnology, 2020. **31**(29): p. 294004.
- 13 32. Mittendorff, M., S. Li, and T.E.J.A.P. Murphy, *Graphene-based waveguide-integrated*
14 *terahertz modulator*. Acs Photonics, 2017. **4**(2): p. 316-321.
15
16
17
18
19
20
21
22
23
24
25
26
27
28
29
30
31
32
33
34
35
36
37
38
39
40
41
42
43
44
45
46
47
48
49
50
51
52
53
54
55
56
57
58
59
60